Biochimica et Biophysica Acta 1838 (2014) 2026–2035

Contents lists available at ScienceDirect

Biochimica et Biophysica Acta

journal homepage: www.elsevier.com/locate/bbamem

A peptide derived from the rotavirus outer capsid protein VP7 permeabilizes artificial membranes

Sarah Elaid [a], Sonia Libersou [b], Malika Ouldali [b], Nelly Morellet [a,1], Bernard Desbat [c], Isabel D. Alves [c], Jean Lepault [b,*], Serge Bouaziz [a,**]

[a] LCRB, CNRS (UMR 8015), Université Paris Descartes, F-75270 Paris, France
[b] LVMS, CNRS (UPR 3296), F-91198 Gif-sur-Yvette, France
[c] CBMN, CNRS (UMR 5248), Université Bordeaux, 33600 Pessac, France

ARTICLE INFO

Article history:
Received 8 November 2013
Received in revised form 2 April 2014
Accepted 7 April 2014
Available online 15 April 2014

Keywords:
Circular dichroism
Plasmon waveguide resonance
ATR-FTIR
NMR
Conformational rearrangement
Membranotropic peptide

ABSTRACT

Biological membranes represent a physical barrier that most viruses have to cross for replication. While enveloped viruses cross membranes through a well-characterized membrane fusion mechanism, non-enveloped viruses, such as rotaviruses, require the destabilization of the host cell membrane by processes that are still poorly understood. We have identified, in the C-terminal region of the rotavirus glycoprotein VP7, a peptide that was predicted to contain a membrane domain and to fold into an amphipathic α-helix. Its structure was confirmed by circular dichroism in media mimicking the hydrophobic environment of the membrane at both acidic and neutral pHs. The helical folding of the peptide was corroborated by ATR-FTIR spectroscopy, which suggested a transmembrane orientation of the peptide. The interaction of this peptide with artificial membranes and its affinity were assessed by plasmon waveguide resonance. We have found that the peptide was able to insert into membranes and permeabilize them while the native protein VP7 did not. Finally, NMR studies revealed that in a hydrophobic environment, this helix has amphipathic properties characteristic of membrane-perforating peptides. Surprisingly, its structure varies from that of its counterpart in the structure of the native protein VP7, as was determined by X-ray. All together, our results show that a peptide released from VP7 is capable of changing its conformation and destabilizing artificial membranes. Such peptides could play an important role by facilitating membrane crossing by non-enveloped viruses during cell infection.

1. Introduction

Non-enveloped viruses, rotaviruses, are the most important cause of severe dehydrating viral gastroenteritis in infants and young children [1]. Rotaviruses are members of the reoviridae family, containing 11 double-stranded RNA gene segments (dsRNA) and replication proteins, VP1 and VP3, within an icosahedral triple-layer particle (TLP) [2]. The 11 dsRNA segments encode the structural proteins (VP1-4, VP6, VP7) and, depending on the strain, five or six non-structural proteins [3]. DsRNA viruses conceal their genome from the innate immune system through the translocation of a high-molecular weight protein-dsRNA complex almost as large as the entire virion by a mechanism that still remains to be experimentally demonstrated. The virion shell contains 780 copies of the predominant glycoprotein VP7, which are assembled into calcium-dependent trimers [4]. Superimposed trimers of VP7 and VP6 constitute a T = 13 l (l for levo) icosahedral lattice [5] defining three types of aqueous channel according to their position with respect to the icosahedral axes of symmetry [6]. VP4 is anchored in the channels surrounding the five-fold axes of the particle and protrudes as a spike by more than 12 nm from the surface of the particle [7,8]. VP6 constitutes the middle layer of the TLP while 120 molecules of VP2 form its innermost layer, obeying a T = 1 icosahedral symmetry, with two molecules in the asymmetric icosahedral unit [9].

The virion must be activated by proteolysis to be infectious [10]. VP4 is cleaved by trypsin, thereby generating the permeabilizing membrane protein VP5* [11,12] and the rotavirus hemagglutinin VP8* [13]. Recently, electron cryomicroscopy (cryoEM) and single-particle analysis at about 4.3 Å resolution showed how the two subfragments of VP4, VP8* and VP5* retain their association after proteolytic cleavage [14].

Abbreviations: dsRNA, double-stranded RNA; CF, carbofluorescein; mOsm, milliOsmol; SA, simulated annealing; TLP, triple-layer particle; DLP, double-layer particle; DPC, dodecylphosphatidylcholine; PWR, plasmon waveguide resonance; ATR-FTIR, attenuated total reflectance-Fourier transformed infrared spectroscopy; CD, circular dichroism; NMR, nuclear magnetic resonance

* Correspondence to: J. Lepault, Laboratoire de Virologie Moléculaire et Structurale, CNRS (UPR 3296), IFR 115, F-91198 Gif-sur-Yvette, France. Tel.: +33 1 69 82 38 55; fax: +33 1 69 82 43 08.
** Correspondence to: S. Bouaziz, Laboratoire de Cristallographie et RMN biologiques, CNRS UMR 8015, 4 Avenue de l'Observatoire, Paris 75270 Paris, France. Tel.: +33 1 53 73 95 78; fax: +33 1 43 26 69 18.
E-mail addresses: Jean.Lepault@vms.cnrs-gif.fr (J. Lepault), serge.bouaziz@parisdescartes.fr (S. Bouaziz).
[1] Present address: ICSN, CNRS (UPR 2301), F-91198 Gif-sur-Yvette, France.

http://dx.doi.org/10.1016/j.bbamem.2014.04.005
0005-2736/

During entry, virions lose their external layer becoming transcriptionally active double-layered particles (DLP). Only viral proteins constitutive of the TLP external layer (VP5*, VP8* and VP7) are thought to be involved in the entry process. Their atomic structure has been determined by X-ray crystallography [15–17]. The trimeric crystal structure of the rhesus rotavirus VP7 bound with the Fab fragment from a neutralizing monoclonal was determined [17]. Each subunit of VP7 folds into two compact domains where each monomer interface binds two calcium ions [17] that maintain the trimeric structure of VP7 and stabilize the outer layer [14,18].

The virion enters the target cell in a multi-step process involving both cellular and viral proteins. VP4 is initially disorganized at the surface of the virus and its proteolytic cleavage generates an organized rod-like spike [7,8] that binds to a receptor at the cell surface. The morphology of the spikes has been described and reveals that the β-barrel domains of two subunits form the body and that of the third one forms the stalk [14]. Several potential receptors have been identified, such as various integrins [19,20] and the heat shock protein Hsc70 [21]. It is not known yet whether human rotavirus VP8* interacts with sialic acid and whether its attachment to the cell involves sialoglycans [22]. However, the surface spike protein VP8* from human rotavirus and the majority of animal rotaviruses interact with the secretor histo-blood group antigens (HBGAs) [23]. It has been suggested that a direct entry into the cell occurs after adsorption onto the cell surface, via the plasma membrane [24], but it seems more likely that rotaviruses enter cells through a dynamin-dependent mechanism based on endocytosis [25]. Isolated VP5* in solution undergoes another structural change, in which three VP5* join together to form a tightly associated trimer [16,26] that binds to lipid bilayers [27] and permeabilizes them [12]. The uncoating of VP7, caused by the removal of calcium, probably accompanies the penetration of the virion and its activation [16].

Membrane-destabilizing peptides are produced by members of different virus families: nodaviridae [28–30], birnaviridae [31,32] and reoviridae [33–35]. In many cases, these peptides were thought to be associated to virus entry [29,31] and a mechanism of pore formation appears to depend on those peptides. While some pores form beta-barrels by assembly of beta-hairpins [34] as many anti-microbial peptides [36] others are formed by α-helices [31]. In all cases, the sequential events constituting the pore formation are not well characterized.

In this work, we identified a domain in the C-terminal region of VP7, predicted to contain a membrane-interacting domain that adopts an amphipathic α-helical structure when inserted into membranes. We showed that this peptide interacts with artificial membranes and renders the membrane semipermeable. Circular dichroism (CD), plasmon waveguide resonance (PWR) and ATR-FTIR spectroscopy were employed to monitor the structure of the isolated peptide, its interaction and its affinity for lipids as well as its orientation in respect to the lipid surface. The solution structure of this domain was determined by nuclear magnetic resonance (NMR) and compared to its corresponding domain in the native protein VP7 [17]. Our data show that this domain undergoes a large structural rearrangement. If ever released from the native protein VP7, this peptide, in association with VP5*, could destabilize membranes and facilitate their permeabilization.

2. Material and methods

2.1. Bioinformatics analysis and peptide synthesis

Membrane domain prediction on the glycoprotein VP7 was performed with the Mpex program (Membrane Protein Explorer), a tool for exploring the topology of membrane proteins by means of hydropathy plots based upon thermodynamics [37] and with the PHD program predicting one-dimensional protein structure by profile-based neural networks [38]. Protein secondary structure prediction was achieved on the full glycoprotein VP7 using the Web server called NPS@ (Network Protein Sequence Analysis, http://pbil.ibcp.fr/NPSA) [39].

2.2. Materials

The identified peptide containing 31 amino acids, and predicted to adopt an alpha helical structure, was extended by 14 and 16 amino acids on the N- and the C-terminal sides respectively to incorporate the predicted β-strands. The obtained peptide with a final size of 61 residues is referred to as $VP7_{61}$. The peptide $VP7_{61}$ from the human rotavirus (B223 strain, Q3ZK60-1 in the Swiss Prot database), purchased from Proteogenics (Oberhausbergen, France), was synthesized by the automated solid phase method with the Fmoc strategy and purified by reverse-phase HPLC.

2.3. Circular dichroism (CD)

CD spectra were recorded at room temperature (20 °C) in a 0.1 cm path length quartz cell on a Jobin-Yvon model C8 spectropolarimeter calibrated with d-camphor-10-sulfonate. The experiments were performed at pH 3.3 and 7.4 with 3 mM of DPC micelles in 1× PBS buffer and the peptide concentration in each sample was 30 μM. Four averaged scans were collected in 0.5 nm interval steps, using an integration time of 2 s and a light bandpass or slit width of 2 nm. Curves were smoothed from 200 to 260 nm using 25 data points. Respective intensities are expressed in mean residue molar ellipticity [θ], calculated from the equation $[\theta] = 100[\theta]_{obs}/CnL$, where $[\theta]_{obs}$ is the observed ellipticity in millidegrees (mdeg), L is the optical path length in centimeters (0.1 cm), C is the final concentration of the peptide in molar and n is the number of amino acid residues.

2.4. Plasmon waveguide resonance (PWR)

PWR experiments were performed on a beta PWR instrument (from Proterion Corp., Piscataway, NJ) that had a spectral angular resolution of 1 mdeg. Resonances can be obtained with light whose electric vector is either parallel (*s*-polarization) or perpendicular (*p*-polarization) to the plane of the resonator surface. The sample to be analyzed (a lipid bilayer membrane) was immobilized on the resonator surface and placed in contact with an aqueous medium, into which the peptides were then introduced. The self-assembled lipid bilayer was formed using a solution (in butanol/squalene, 0.93:0.07, v/v) of 8 mg/ml egg phosphatidylcholine (Avanti Polar Lipids). The method used to prepare the lipid bilayer is based on the procedure by Mueller and Rudin [40] to make black lipid membranes cross a small hole in a Teflon block: the method has been reported [41,42]. The buffer used for the experiments was Tris-buffer (10 mM Tris 0.1 M NaCl, 2 mM EDTA, pH 7.6). Because the peptide was not completely soluble in the Tris buffer, 5% DMSO was added to the 1 mM solution of peptide. After bilayer formation, the peptide was incrementally added to the cell sample compartment and the spectral changes were monitored with both polarizations. It should be noted that DMSO perturbs the lipid bilayer, therefore a control experiment was performed using the same final DMSO concentration used for each peptide solution injected into the cell. The shifts obtained upon DMSO addition were subtracted from those obtained upon peptide addition to the lipid bilayer. Affinities between the peptide and the lipids were obtained by plotting the PWR spectral changes that occur upon incremental additions of ligand to the cell. Data fitting (GraphPad Prism) through a hyperbolic saturation curve provides the dissociation constants. It should be noted that concomitantly with the binding process other processes such as membrane reorganization and solvation occur and thus the dissociation constants correspond to apparent dissociation constants. Spectral simulation [41] and/or graphical analysis [43] allows one to obtain information about changes in the mass density, structural asymmetry and molecular orientation induced by bimolecular interactions occurring at the resonator surface. Here, the graphical analysis method was employed. Briefly, this method consists of deconvoluting the components of the PWR spectra that are due to changes in mass in the lipid film from those that are due to changes in structural

anisotropy. The method has been thoroughly described before and will not be further described here [43]. Such distinction can be done based on the magnitude and direction of the PWR spectra shifts observed for the *s*- and *p*-polarized light. The method has been employed to analyze the interaction of peptides with lipid membranes [31,44–46].

2.5. ATR-FTIR spectroscopy

Infrared spectra were recorded with a Nicolet 6700 FT-IR spectrometer (Nicolet Instrument, Madison, WI) equipped with a liquid nitrogen cooled mercury–cadmium–telluride detector. Lipid bilayers were formed by the fusion of SUVs onto the ATR germanium crystal of a Miracle Cell (Spike Technology). Ten microliters of 3 mg/mL EggPC SUVs lipid solution in PBS buffer were deposited on the crystal via the Teflon cell at room temperature. After 10–15 min, the non-adsorbed lipids were rinsed 5 times with 20 μL of PBS buffer, and finally 20 μL of PBS buffer were added in the Teflon cell before the polarized *s*- and *p*-ATR-FTIR spectra were recorded. The polarized spectra were obtained using a motorized rotating wire-grid polarizer. Once the bilayer was formed, the peptide was injected in the solution to reach 1 μM. The ATR spectra were recorded at room temperature and 800 scans at 8 cm^{-1} spectral resolution were co-added.

2.6. Fluorescence assay

Liposomes containing carboxyfluorescein (CF) were prepared as previously described [11]. The release of CF after addition of the peptide was monitored by assessing the increase in fluorescence at 520 nm, with excitation at 492 nm in a thermostatically controlled Perkin-Elmer LS50B spectrofluorimeter. The value for 100% release was obtained by adding Triton X-100 at the end of the reaction. All fluorescence experiments were carried out at least three times. The fluorescent probe used in the experiments, CF, has an extra carboxyl group relative to fluorescein, making the molecule more polar and less capable of crossing membranes at pH 7.4 at low phosphate buffer concentration [47]. Thus all fluorescence assay experiments were conducted at pH 7.4, because at this pH the effect on passive diffusion of CF through the membrane liposomes is weak.

2.7. Sample preparation for NMR experiments

For NMR sample preparation, 4.4 mg of $VP7_{61}$ was dissolved in a $CD_3OH/CDCl_3$ (1:1, v/v) mixture or in 500 μl of water with 100 mM of dodecylphosphatidylcholine (DPC) to give a 1 mM final concentration of the peptide at pH 3.3. NMR experiments were performed at various temperatures ranging from 293 K to 323 K on an AVANCE Bruker spectrometer operating at 600.13 MHz. Phase-sensitive ^1H DQF-COSY [48] and TOCSY [49] experiments with a 70 and 80 ms spin lock duration were recorded. NOESY experiments [50] were performed at three different mixing times of 100, 200 and 250 ms. Experiments were recorded with a 7788.16 Hz spectral width, 2048 real points in t2, and 512 t1-increments. A π/6 phase-shifted sine bell window function was applied prior to Fourier transformation in both dimensions (t1 and t2). The temperature was controlled externally with a Bruker BCU 05 chiller. Data were processed with Topspin 1.3 software (Bruker) and analyzed with SPARKY (T.D. Goddard and D.G. Kneller, UCSF, San Francisco, CA) or CcpNmr Analysis [51].

2.8. Assignment and structure calculation

All proton resonances were assigned by a widely described homonuclear 2D NMR spectroscopy strategy [52] based on the identification of individual amino-acid spin systems revealed by the DQF-COSY and the TOCSY experiments. In a second step, the amino-acid spin systems were correlated through the information extracted from the NOESY spectra performed at different mixing times.

The structure of $VP7_{61}$ in $CDCl_3/CD_3OH$ (1:1, v/v) was determined by using the distance restraints obtained from Nuclear Overhauser Effect (NOE) cross-signal volumes measured on the NOESY spectra recorded at 293 K with 100 ms and 200 ms mixing time. Peaks were integrated and converted into distances on the basis of an r^{-6} dependence, with a tolerance of 20%. Distances were calibrated using cross-peaks between the aromatic protons (Hδ, Hε) of Y323 and Y324, which have a known distance of 2.45 Å. Distance geometry and simulated annealing regularization were performed to embed and optimize the initial structures using the software XPLOR-NIH [53]. The 20 best structures generated in 100 attempts at embedding and optimization were selected based on satisfactory covalent geometry, low distance restraint violations and favorable non-bonded energy. These structures were further optimized by restrained molecular dynamics, in vacuum, with a distance-dependent dielectric constant, as previously described [54], and were evaluated for stereochemical quality by PROCHECK-NMR [55].

The structure calculation of $VP7_{61}$ in DPC was performed with CNS version 1.2 [56] using ARIA v.2.3 [57], from manually assigned ^1H-^1H restraints derived from 200 and 250 ms mixing time NOESY spectra at 323 K. The standard annealing protocols were used, including NOE distance calibration. The starting structures were generated based on a linear template molecule with randomly associated velocities for all atoms. For iterations 1–7, 200 structures were calculated and the NOE distance restraints were recalibrated by ARIA based on the 100 lowest energy structures. The violation tolerance was progressively reduced to 0.1 Å in the last iteration (iteration 8), in which 80 structures were calculated. For the structure calculations, a five-stage simulated annealing (SA) protocol was used employing cartesian dynamics. The high-temperature stage consisted of 10,000 steps at 10,000 K, followed by three cooling stages: 4000 steps to 2000 K, 5000 steps to 1000 K and 4000 steps to 50 K. During the SA protocol the force constant for the NOE restraints was set to 0, 10 and 50 kcal mol^{-1} $Å^{-2}$. The final 80 structures were then refined in a shell of water molecules and the eight best structures were analyzed as the final structure ensemble. The Ramachandran plot statistics of the final structure ensemble was analyzed with the PROCHECK software.

2.9. Accession numbers

The ^1H NMR resonance assignments of $VP7_{61}$ identified in $CDCl_3/CD_3OH$ (1:1, v/v) and in DPC have been deposited at the Biological Magnetic Resonance Data Bank under accession codes RCSB101627 and RCSB102553 respectively. The coordinates of the structures calculated in $CDCl_3/CD_3OH$ (1:1, v/v) and in DPC have been deposited at the Protein Data Bank (PDB) with accession codes 2KVL and 2LM7 respectively.

3. Results

3.1. A domain in the C-terminal region of VP7 is predicted to adopt an amphipathic helical structure

Several peptides derived from VP7 have been shown to interact with membranes and destabilize them [58]. We have used bioinformatics tools to identify a potential membranotropic domain within VP7, capable of destabilizing artificial membranes. The full sequence of VP7 was submitted to secondary structure prediction [37,38,59] and was predicted to contain a membrane domain overlaying residues W292-M310 in its C-terminal region (Fig. 1A). Moreover, an α-helix spanning residues Q280-M310 and two extended strands L269-I271 and S321-Y324 were predicted to be surrounded by unstructured loops (Fig. 1B). The predicted helical membrane domain Q280-M310 was shown to have amphipathic properties in a helical wheel representation with the hydrophilic residues on one side (blue) and the hydrophobic ones (red) on the other side (Fig. 1C). This peptide was thus extended by 14 and 16 amino acids on the N- and the C-terminal sides respectively to include all predicted

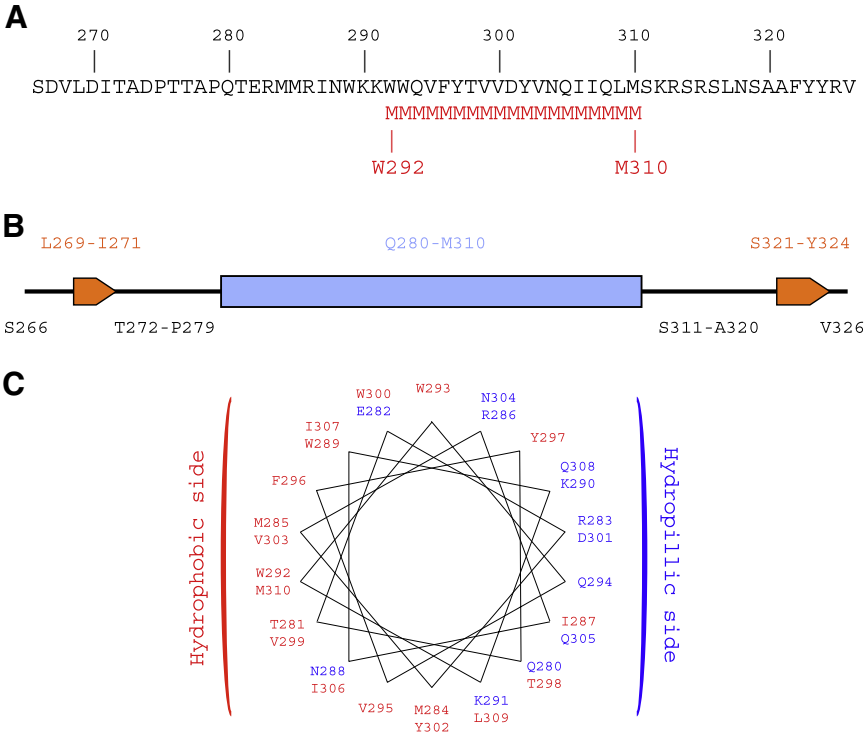

Fig. 1. Prediction of an amphipathic alpha helix in the C-terminal region of VP7 by a combination of Bioinformatics tools predicting membrane domains [37] and secondary structure elements [39]. (A) The full sequence of VP7 submitted to the program Mpex [37] predicted a potential membrane domain spreading residues W292-M310. (B) The full sequence of VP7 was submitted to the Web server NPS@ (Network Protein Sequence Analysis, http://pbil.ibcp.fr/NPSA) [39], which predicted an alpha helix covering residues Q280-M310 and two extended strands L269-I271 and S321-Y324 surrounded by unstructured loops. (C) Helical wheel representation showing that the domain Q280-M310 is predicted to adopt an alpha helical structure with amphipathic properties.

secondary structures. The peptide has therefore a final size of 61 residues and is referred to hereafter as $VP7_{61}$.

3.2. Circular dichroism shows that $VP7_{61}$ adopts an alpha helical structure in DPC

CD spectra of $VP7_{61}$ were performed at pH 3.3 and pH 7.4 at a concentration of 30 μM, in DPC micellar suspension with a 1/100 peptide/lipid ratio (Fig. 2). The spectra of $VP7_{61}$ in 3 mM membrane-mimicking agent DPC, at pH 7.4 (Fig. 2; red spectra) and at pH 3.3 (Fig. 2; blue spectra) present the characteristic negative bands at 209 nm (parallel π → π* transitions) and at 222 nm, indicating the formation of an α-helix. The part of the spectra containing the maximum at 190 nm is not represented because the signal was saturated by the presence of NaN_3 in the PBS buffer. The two pHs 3.3 and 7.4 have been chosen to demonstrate that the peptide $VP7_{61}$ adopts an alpha helical structure whatever the pH. Actually, the helical content seems to be higher at pH 7.4 compared to pH 3.3 since a lower ellipticity value is measured at acidic pH.

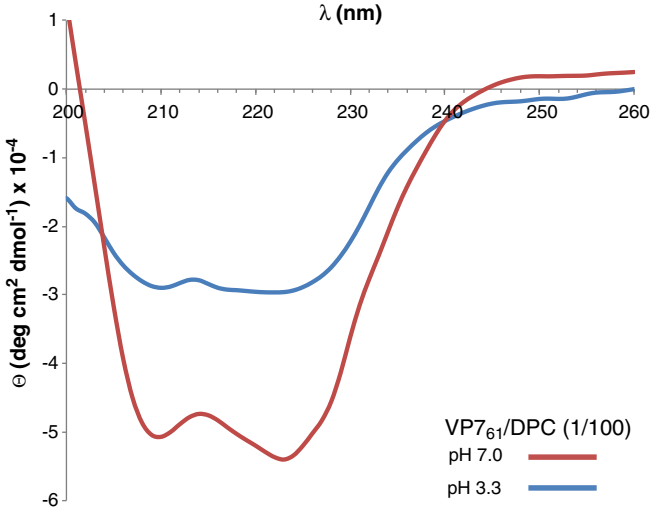

Fig. 2. Circular dichroism spectra of $VP7_{61}$. The spectrum of $VP7_{61}$ (red) in the presence of membrane-mimicking agents such as DPC with a peptide/lipid ratio 1/100 at pH 7.4, presents the same typical α-helix structure as at pH 3.3 (blue).

3.3. $VP7_{61}$ interacts with artificial membranes

PWR was used to follow the interaction of $VP7_{61}$ with the lipid bilayer in terms of affinity and changes induced by the peptide on the lipid bilayer organization and total mass. The addition of $VP7_{61}$ to an egg PC bilayer led to positive spectral shifts for both *p*-polarization (+14 mdeg) and *s*-polarization (+13 mdeg) (Fig. 3A and B), indicating an increase in the refractive index of the system. This is a natural consequence of the increase in mass due to peptide interaction, which can also be associated with a mass increase coming from the reorganization of the lipid induced by the peptide. The magnitudes of the changes are comparable to other studies regarding membrane active peptides [46,60,61]. Washing the PWR cell compartment with buffer does not lead to the original spectra of the lipid bilayer prior to peptide addition and thus, the spectral changes induced by the peptide are non-reversible. From the resonance minimum position as a function of concentration an apparent dissociation constant was determined (details can be found in Section 2, Material and methods section) and a K_D of 95 nM was obtained (Fig. 3C). A graphical analysis of the spectral shifts observed upon peptide interaction with the membrane indicates that 90% of the spectral changes are due to changes in mass of the system and the remaining 10% are due to changes in structure (details on graphical analysis method are provided in Section 2, Material and methods and in Ref. [43]). Additionally the spectral changes

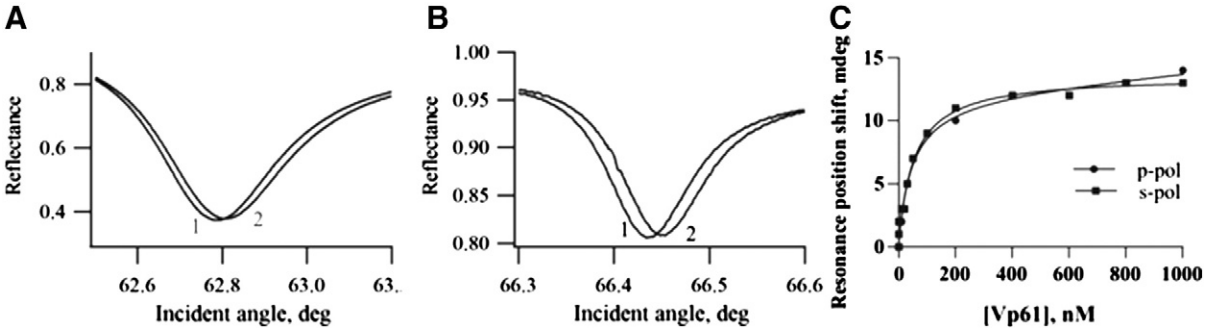

Fig. 3. PWR spectra of the interaction of $VP7_{61}$ with an egg PC lipid bilayer. PWR spectra (A and B) obtained for the lipid bilayer before (1) and after (2) addition of $VP7_{61}$ to the bilayer were obtained for *p*- and *s*-polarized light, respectively. The resonance position shifts obtained for *p*- (●) and s- (■) polarizations for the incremental addition of $VP7_{61}$ are represented, and so is the hyperbolic binding curve (C) from which a K_D value of 95 nm was obtained.

observed for peptide addition are quite similar for both polarizations indicating that similar changes occur in the plane of the lipid bilayer and off plane.

3.4. $VP7_{61}$, interacting with an EggPC bilayer, folds in an α-helix structure

Polarized ATR infrared spectra of the $VP7_{61}$ peptide in contact with EggPC bilayer were recorded. The noise is present outside the region of interest for the assignment of secondary structures and therefore these spectra are of sufficient quality to be able to assign secondary structures with certainty. This noise level is normal especially given the low signal absorption as our group has already published on other peptides [62]. The peptide was detected by the presence of the Amide I band between 1700 cm^{-1} and 1600 cm^{-1} and the amide II band around 1550–1540 cm^{-1} (Fig. 4). The amide I band was centered at 1654 cm^{-1} which indicates that the peptide is mainly folded in an α-helix structure. However, other secondary structures are also present such as a turn defined by a band at 1675 cm^{-1} and a β-sheet defined by a band at 1633 cm^{-1} clearly observed on the *p*-polarized spectrum (Fig. 4). The presence of the various structures makes it difficult to determine the peptide orientation from the dichroic ratio of the bands. However, the large intensity of the amide I in *p*-polarization suggests that the peptide folds in an α-helix with a trans membrane orientation.

3.5. $VP7_{61}$ induces membrane destabilization

The release of fluorescent molecules from the liposomes containing quenched carboxyfluorescein increased strongly upon the addition of $VP7_{61}$ (Fig. 5), revealing the release of the carboxyfluorescein from the liposomes. Both speed and magnitude of liposome destabilization depended on the concentration of $VP7_{61}$ and the increase in fluorescence reached saturation at micromolar concentrations of $VP7_{61}$. Particular solvent conditions were used in order to prevent $VP7_{61}$ tendency to aggregate or oligomerize in aqueous solutions. Indeed, the peptide was solubilized in DMSO (at high concentration) and diluted with buffer for the various experiments. At low nanomolar concentrations, $VP7_{61}$ leads to a significant leakage of the liposomes whereas DMSO does not (Fig. 5).

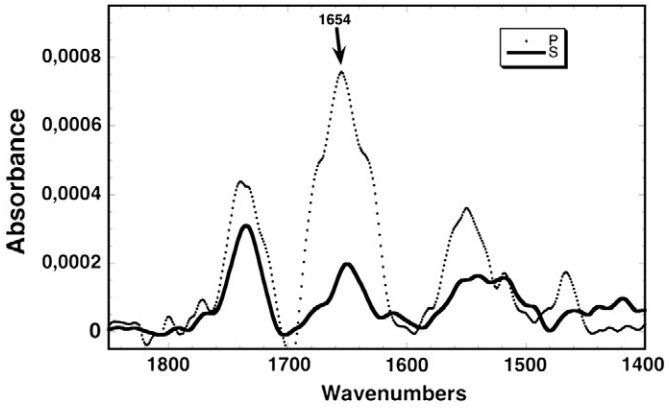

Fig. 4. ATR-FTIR spectroscopy of $VP7_{61}$ in interaction with an egg PC lipid bilayer. Polarized ATR infrared spectra of the $VP7_{61}$ peptide with bilayer of EggPC lipids is reported. The peptide was detected by the presence of the Amide I band between 1700 and 1600 cm^{-1} and the amide II band around 1550–1540 cm^{-1}. The amide I band centered at 1654 cm^{-1} indicates that the peptide is mainly folded in α-helix. However, turn (1675 cm^{-1}) and beta-sheet (1633 cm^{-1}) structures are also present and clearly observed on the *p*-polarized spectrum.

3.6. Solvent condition optimization for the structural study of $VP7_{61}$

The structure of the native glycoprotein VP7 containing the domain $VP7_{61}$ in its C-terminal region is known [17]. The solvent conditions to solubilize the peptide $VP7_{61}$ were determined and optimized by monitoring the quality of the signal by 1D proton NMR (Fig. 6). The line broadening of the resonances on the 1D proton NMR spectra of $VP7_{61}$ in 100% H_2O, confirmed that the peptide had a strong tendency to aggregate in aqueous solutions (Fig. 6A). To overcome this problem, $VP7_{61}$ was analyzed in a $CDCl_3/CD_3OH$ (1:1, v/v) condition (Fig. 6B) and in the presence of variable amounts of DPC (Fig. 6C–E) that were previously shown to mimic the hydrophobicity of the membranes [63–65], at different temperatures (Fig. 6E–G). Thus, it was possible to perform 2D NMR studies of $VP7_{61}$ solubilized in $CDCl_3/CD_3OH$ (1:1, v/v) at 293 K or in 100 mM DPC at 323 K. Despite the circular dichroism experiments revealed a lower ellipticity value and lower helical content at pH 3.3 compared to pH 7.4, an acidic pH was chosen to work with DPC. At this acidic pH the amide proton exchange rate is slower than that at a pH close to the neutrality. In case the peptide has a strong tendency to aggregate and because we are working in the presence of micelles, it allows getting a sharper signal and more intense peaks that facilitate the interpretation of the NMR spectra. Another reason is that at physiological pH, acidic and basic residues are negatively and positively charged, respectively. The intermolecular interactions between these charges lead to an aggregation of the peptide. At acidic pH, the protonation of the basic and acidic residues prevents intermolecular interactions.

3.7. Proton NMR chemical shift assignment

The complete proton chemical shift assignment was achieved (Supplementary data Fig. S1 and Supplementary data Tables S1) in $CDCl_3/CD_3OH$ (1:1, v/v) at 293 K and in 100 mM DPC at 323 K (Supplementary data Fig. S2 and Supplementary data Table S2). Characteristic signals showed that, in both conditions, the peptide was organized into two helical domains spanning residues Q280-M310 and R315-Y324 in $CDCl_3/CD_3OH$ (1:1, v/v) (Supplementary data Fig. S3A) and residues T281-M310 and S316-F322 in DPC (Supplementary data Fig. S3B). In both solvents, the first helix is flanked by two flexible regions S266-P279 and S311-S314 in $CDCl_3/CD_3OH$ (1:1, v/v)

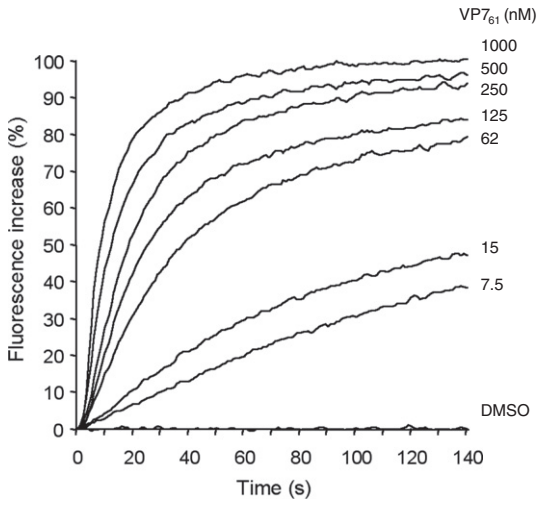

Fig. 5. Membrane destabilization by VP7$_{61}$. The peptide VP7$_{61}$ strongly destabilizes artificial membranes and releases the fluorescein contained in liposomes by perforating their membranes. The increase in fluorescence reached saturation at micromolar concentrations of VP7$_{61}$ and depended on the concentration of VP7$_{61}$.

(Supplementary data Fig. S3A) and S266-Q280 and S311-R315 in a DPC environment (Supplementary data Fig. S3B). These results show that a hydrophobic environment is necessary for peptide folding.

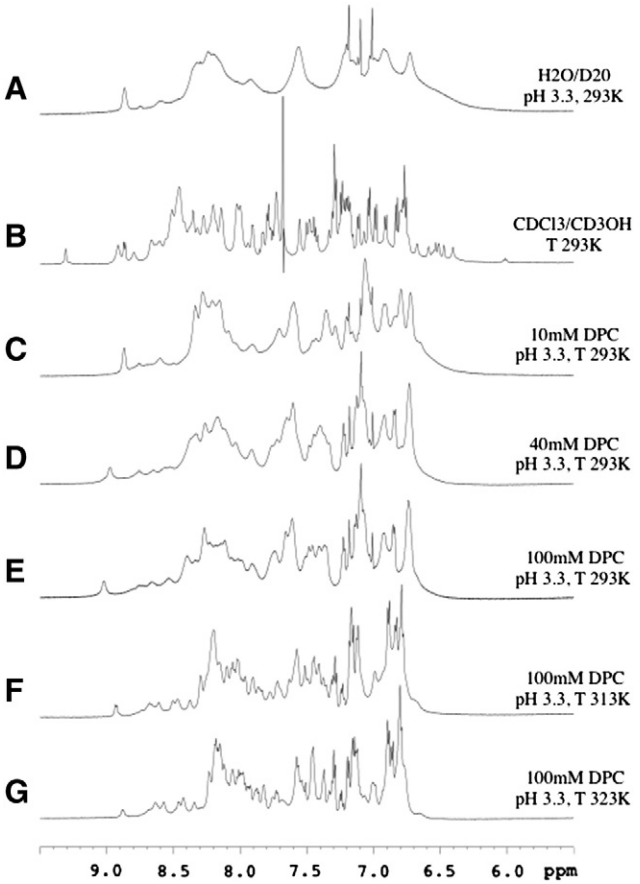

Fig. 6. Solubilization of VP7$_{61}$ followed by 1D proton NMR. Only the amide and aromatic proton region is represented. (A) In pure water at pH 3.3, the peptide appears to be aggregated with large line broadening. (B) In a mixture of $CDCl_3/CD_3OH$ (1:1, v/v), the peptide seems to be structured with a large spreading of the chemical shifts. (C–E) The peptide is structured when solubilized with increasing DPC concentrations (10 mM, 40 mM and 100 mM) at the temperature of 293 K and pH 3.3. (F–G). By increasing the temperature to 323 K the quality of the signal is increased with a narrow linewidth.

3.8. Structure of VP7$_{61}$ in $CDCl_3/CD_3OH$ (1:1, v/v)

The structure of VP7$_{61}$ in $CDCl_3/CD_3OH$ (1:1, v/v) was determined using the hybrid distance geometry-simulated annealing method implemented in XPLOR 3.84 [53,56,66]. Out of 100 calculated structures, 10 were selected according to their low overall energy and their low number of distance violations. The refined structure of VP7$_{61}$ exhibits two α-helical domains. The first one, Q280-M310, is flanked by an unstructured region S266-P279 and a flexible turn S311-S314, and the second one, R315-Y324, shows various orientations related to the first one (Fig. 7A). The calculated structures of VP7$_{61}$ are of good quality, with a high degree of convergence (Table 1). The first α-helix encompassing amino acids Q280-M310 has an average rmsd of 0.81 ± 0.31 Å calculated on the backbone atoms, while the second α-helix R315-Y324 has an average rmsd of 0.47 ± 0.12 Å. None of the structures exhibited a distance violation greater than 0.2 Å and all of them presented a good covalent geometry. The distribution of the ϕ, Ψ angles revealed that 76.3%, 20% and 3.7% of the residues were respectively found in the favored, additional and generously allowed regions and that none of the ϕ, Ψ angles were located in non-favorable regions (Table 1). The analysis of the largest helical domain Q280-M310, according to the nature of the amino acid side chains, shows a hydrophilic side formed by residues Q280, R283, R286, K290, K291, Q294, Y297, D301, Q305, Q308 and a hydrophobic one composed by residues T281, M284, M285, W289, W292, W293, F296, V299, V300, V303, I306, I307, M310. These two sides define an amphipathic helix (Fig. 7B).

3.9. Structure of VP7$_{61}$ in micelle environment

In a second step, the structure of VP7$_{61}$ was studied by NMR in DPC micelles. Because of their zwitterionic head, DPC mimics well the cell

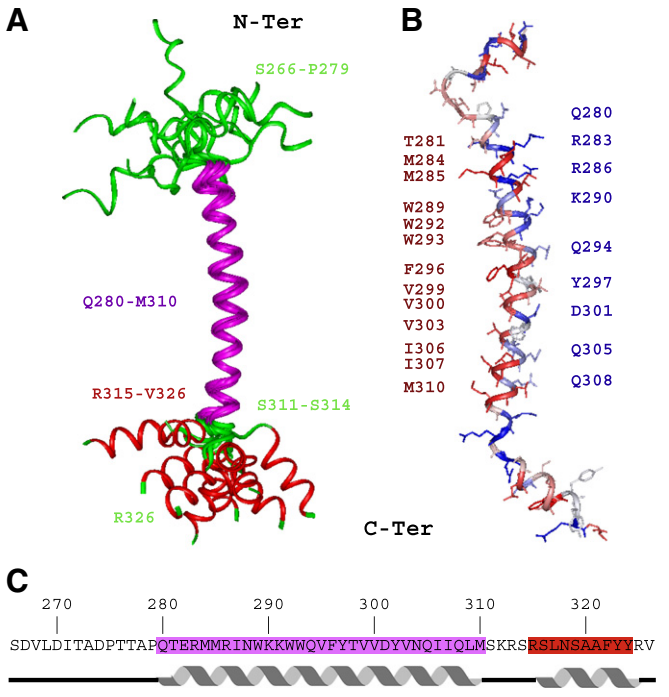

Fig. 7. NMR structure of VP7$_{61}$ in $CDCl_3/CD_3OH$ (1:1, v/v). (A) Superimposition of the 10 energetically most favorable structures of VP7$_{61}$ calculated using XPLOR-NIH [53]. Two α-helical domains characterize the structure. The first one, Q280-M310, is flanked by one unstructured region S266-P279 and a flexible turn S311-S314 followed by the second well defined domain (R315-Y324). (B) Helix Q280-M310 shows amphipathic properties with one hydrophobic face constituted by residues T281, M284, M285, W289, W292, W293, F296, V299, V300, V303, I306, I307 and M310, colored in red and a hydrophilic face formed by residues Q280, R283, R286, K290, K291, Q294, Y297, D301, Q305 and Q308, colored in blue. (C) Secondary structures identified within VP7$_{61}$ in $CDCl_3/CD_3OH$ (1:1, v/v) from the analysis of the observed medium range NOEs.

Table 1
NMR restraints and structural statistics.

	$CD_3OH/CDCl_3$		DPC	
NMR derived distance restraints				
Total	765		887	
Intraresidue	363		563	
Sequential ($\|i-j\| = 1$)	159		213	
Medium-range ($1 < \|i-j\| \leq 4$)	145		111	
Long-range ($\|i-j\| > 5$)	0		0	
Hbonds	98			
Distance violations				
(>0.2 Å)	0		0	
r.m.s.d.				
From experimental distance restraints (Å)	$(1.212 - 1.328)\times10^{-2}$		$(1.348 - 2.077)\times10^{-2}$	
From idealized geometry				
Bonds (Å)	$(1.222 - 1.458)\times10^{-3}$		$(2.718 - 3.095)\times10^{-3}$	
Angles (deg)	(0.468 − 0.476)		(0.417 − 0.488)	
Improper angles (deg)	(0.334 − 0.336)		(0.934 − 1.145)	
Potential energies (Kcal/mol)				
E_{NOE}	(5.434 − 1.812)		(8.067 − 19.138)	
E_{VDW}	(0.692 − 8.607)		((−89.964) − (−170.835))	
E_{BOND}	(1.560 − 2.221)		(7.712 − 10.003)	
E_{ANGLES}	(62.742 − 64.763)		(49.698 − 68.099)	
$E_{IMPROPERS}$	(9.617 − 9.783)		(20.298 − 28.1813)	
E_{TOTAL}	(80.047 − 87.189)		((−1902.57) − (−1763.29))	
Ramachandran analysis of residues				
Favored region (%)	76.3%		72.60%	
Additional allowed regions (%)	20.0%		23.00%	
Generously allowed regions (%)	3.7%		2.21%	
Disallowed regions (%)	0%		2.19%	
r.m.s.d. on the backbone atoms (Å)				
	To mean structure	Pairwise	To mean structure	Pairwise
Q280-M310	0.81 +/- 0.31	1.13 +/- 0.40		
R315-Y324	0.47 +/- 0.12	0.36 +/- 0.13		
Q280-M310/R315-Y324	3.35 +/- 1.10	3.84 +/- 1.01		
Q280-Y324	3.44 +/- 1.00	3.95 +/- 0.99		
E282-M310			0.73 +/- 0.25	1.10 +/- 0.37
L317-F322			2.26 +/- 0.14	0.79 +/- 0.28
E282-M310/L317-F322			3.73 +/- 1.53	6.86 +/- 2.40
E282-F322			3.98 +/- 1.38	5.40 +/- 2.12

membrane hydrophobic environment and facilitates NMR studies by solubilizing efficiently hydrophobic or amphipathic α-helices. $VP7_{61}$ was solubilized in the presence of 10 mM DPC and then incremented amounts of DPC were added at 293 K until the 1D spectrum indicated that equilibrium of $VP7_{61}$ structure in micelles was reached (Fig. 6C–E). The temperature was then increased from 293 K to 323 K, which allowed obtaining a narrower line width (Fig. 6E–G). The analysis of the identified medium range NOEs in DPC confirmed that $VP7_{61}$ is organized in two helical domains with characteristic NOEs found for the two stretches T281-I307 and S316-S319 (Supplementary data Fig. S3B), as observed in $CDCl_3/CD_3OH$ (1:1, v/v) (Supplementary data Fig. S3A). The structure of $VP7_{61}$, calculated using the NMR restraints collected for the peptide in 100 mM DPC and at 323 K, is characterized by one helical domain spanning residues T281-M310, followed by an unstructured domain S311-R315 and ended by a second α-helix S316-F322 (Fig. 8). The first helix T281-M310 is well defined with an average rmsd of 0.73 (±0.25) Å calculated on the backbone atoms for the eight best structures (Table 1 and Fig. 8A). The helix T281-M310 has amphipathic characteristics with the amino acid side chains of R283, R286, K290, Q294, Y297, D301, Q305, and Q308 forming a hydrophilic surface while the residues T281, M285, W289, W293, F296, V300, V303, I306, and M310 provide an uninterrupted hydrophobic one (Fig. 8B). The C-terminal α-helix S316-F322 is less well-defined in the presence of DPC (Fig. 8C) than its counterpart R315-V326 in $CDCl_3/CD_3OH$ (1:1, v/v) (Fig. 7C).

3.10. $VP7_{61}$ adopts a different structure when compared to its counterpart in the whole VP7 protein

The structure of the $VP7_{61}$ domain, determined by NMR was then compared to that of its counterpart in the X-ray structure of the native VP7 [14,17], for which most of the polypeptide chain was determined, giving an atomic model extending from residue 78 to residue 312. The counterpart of $VP7_{61}$ in the X-ray structure of VP7 adopts a conformation consisting of a short β-sheet, β13 M284-I287 (in cyan Fig. 9A), and an α-helix W292-M310 with a kink in its center between residues D301 and Y302 (in magenta Fig. 9A) while the C-terminal domain of VP7 spanning residues S316 to V326 is not observable and thus undefined (Fig. 9A). Thus, the NMR structure of $VP7_{61}$ containing two α-helical domains T281-M310 and S316-F322, does not exhibit the same 3D organization (Fig. 9B). The structure of the peptide $VP7_{61}$ evolves depending on whether it is embedded in the native protein VP7 (Fig. 9A) or in its isolated form (Fig. 9B). The alignment of the sequences and secondary structures are shown in Fig. 9C.

4. Discussion

Non-enveloped viruses, as rotaviruses, destabilize the host cell membrane by processes that remain hypothetical although it is known that the two outer capsid proteins VP4 and VP7 are involved at different levels in

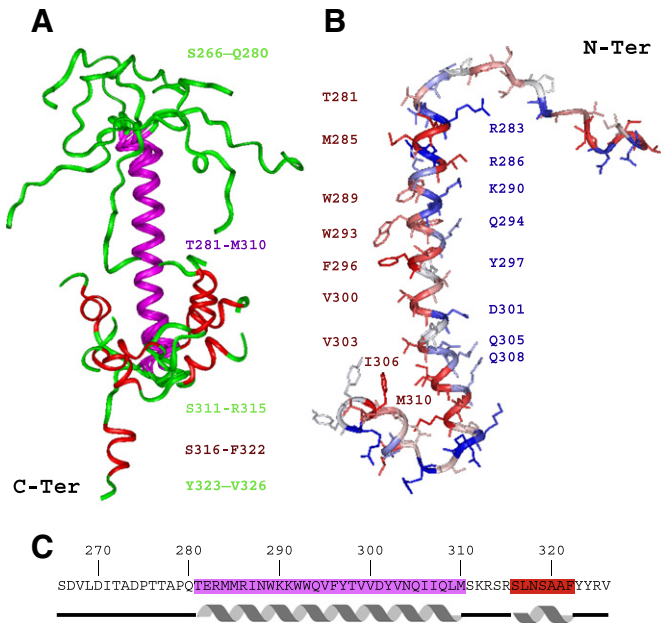

Fig. 8. NMR structure of $VP7_{61}$ in DPC. (A) Superimposition of the eight energetically most favorable structures of $VP7_{61}$ calculated with ARIA. The structure is characterized by two α-helical domains, T281-M310 and S316-F322, separated by a flexible region S311-R315. The first helix is preceded by an unstructured region, S266-Q280. (B) Helix T281-M310 shows amphipathic properties with one hydrophobic face constituted by residues M285, W289, W293, F296, V300, V303, I306 and M310, colored in red and a hydrophilic face formed by residues R283, R286, K290, Q294, Y297, D301, Q305 and Q308, colored in blue. The second helix S316-F322 in DPC is shorter than its counterpart R315-Y324 in $CDCl_3/CD_3OH$ (1:1, v/v). (C) Secondary structures identified within $VP7_{61}$ in DPC from the analysis of the observed medium range NOEs.

both virus attachment and in cell entry. Both VP4 and VP7, contain motifs for binding members of the heterodimer α/β integrin family [20,67] and the heat shock protein Hsc70 to lipid rafts [21]. The two viral proteins VP4 and VP7 induce neutralizing antibodies that block rotavirus entry [68], and the uncoating of VP7 is necessary for the final steps of DLP delivery [69,70]. Moreover, the ESCRT complex seems to play a role in the entry of the human and simian rotavirus in epithelial cells [71]. Independent of the molecules recognized for attachment to the cell and whatever the endocytic pathway followed, rotaviruses converge in early endosomes and use multivesicular bodies to penetrate the cells [71]. But ultimately, the mechanism by which the rotavirus enters the cell remains unknown.

The native protein VP7 is unable to destabilize or permeabilize biological or artificial membranes. Here, using bioinformatics tools, we show that, on the contrary, VP7 contains a domain, $VP7_{61}$, that is able to destabilize or permeabilize membranes. When different concentrations of $VP7_{61}$ are added to liposomes containing carboxyfluorescein, the release of this fluorescent molecule is observed, indicating loss of membrane integrity (e.g., pore formation).

The interaction of $VP7_{61}$ with an egg PC bilayer studied by PWR indicates that 90% of the spectral changes are due to changes in mass of the system with an apparent dissociation constant $K_D = 95$ nM. This could represent the first steps of the interaction between the perforating peptide $VP7_{61}$ and the membrane. The spectra obtained by ATR-FTIR spectroscopy on the domain $VP7_{61}$ can be compared with the ATR spectra published on the hΦ20 peptide [72], consisting of 20 alternating alanine and leucine residues and two flanking lysines at each terminus, in interaction with POPC (lipid 1-palmitoyl-2-oleoyl-sn-glycero- 3 phosphocholine) bilayer. The hΦ20 peptide was mainly in α-helix and the relative intensities of the amide I and amide II bands are similar to those observed with the $VP7_{61}$ peptide. This is especially true for the *s*-polarization spectra where the amide I and amide II bands have

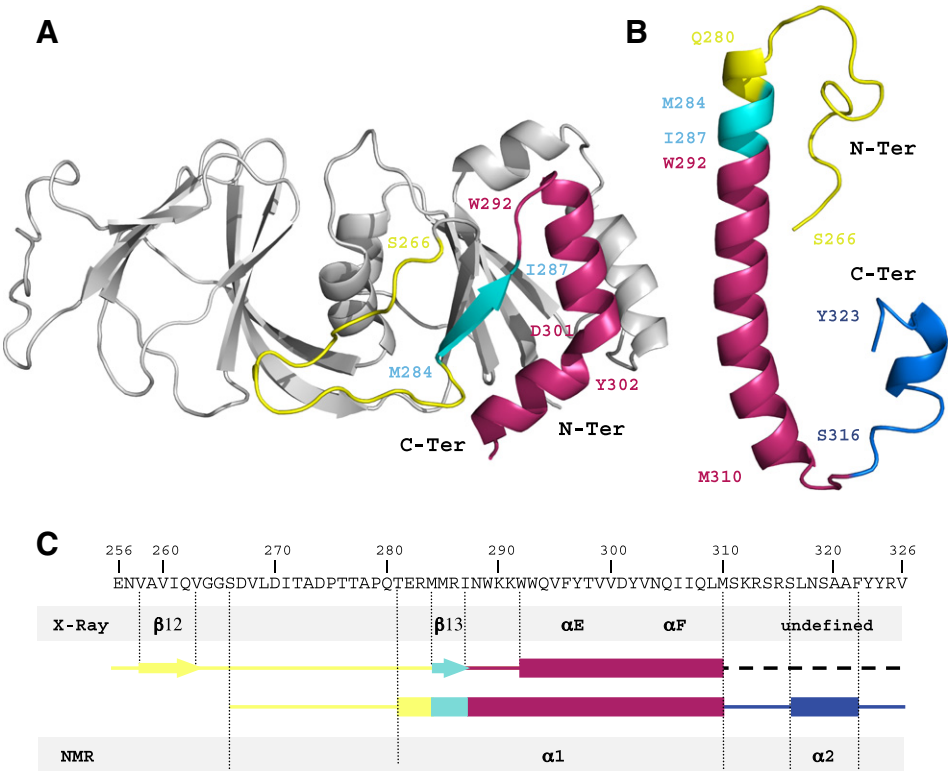

Fig. 9. Comparison of the NMR structure of the C-terminal domain $VP7_{61}$ with its X-ray structure counterpart. (A) X-ray structure of the native protein VP7. (B) Structure of $VP7_{61}$ as determined by NMR in this study in a micellar environment. The corresponding domains in the X-ray structure and in the NMR structure, S266-R283, M284-I287, N288-M310, and R311-V326, are colored in yellow, cyan, red and blue respectively. (C) Comparison of the secondary structures in the C-terminal domain of VP7 determined by X-ray crystallography and NMR.

almost the same intensities. From these data, an angle of 33° with respect to the normal membrane was evaluated for the hΦ20 peptide [72]. One could hypothesize that a similar angle is formed for $VP7_{61}$ helical part. Due to the fact that $VP7_{61}$ adopts other structures (although in minority) than α-helix, this angle cannot be determined.

Circular dichroism and NMR structural studies in the presence of DPC, a membrane-mimicking agent, showed that $VP7_{61}$ is predominantly organized into two alpha helical domains. The properties of the peptide $VP7_{61}$ are mainly due to the presence of an amphipathic α-helix Q280-M310 identified in its three-dimensional structure. The amphipathic properties of this domain explain its tendency to aggregate in polar solvents and account for its ability to interact with biological and artificial membranes. Many amphipathic α-helical structures are known to aggregate at the membrane surface, to insert into biological membranes, to form pores and to destabilize them [73,74].

Spectroscopic methods as NMR experiments performed in micelle environment or in $CDCl_3/CD_3OH$ (1:1, v/v), circular dichroism achieved at two different pHs or polarized ATR infrared spectroscopy revealed that the isolated peptide $VP7_{61}$ folded into an alpha helical structure with amphipathic properties. Moreover we showed that the $VP7_{61}$ domain structure depends on its environment, and that the isolated peptide and the peptide embedded in the native protein adopt different structures (NMR and X-ray data, respectively). The 3D structure of $VP7_{61}$, as determined by NMR (Figs. 8 and 9B) in a DPC environment, is different from its counterpart domain in the X-ray structure of VP7 bound to the Fab fragment of a neutralizing monoclonal antibody [17] (Fig. 9A). The main differences consist firstly in a strand M284-I287 involved in a β-sheet in the X-ray structure of VP7, that switches into an α-helical conformation in $VP7_{61}$. Secondly, the helix T281-M310 identified in the NMR structure is larger than the corresponding domain W292-M310, in the X-ray structure, where a kink splits the helix into two helical subdomains W292-D301 and Y302-M310. Thirdly, the S311-V326 domain, undefined in the X-ray structure of VP7, adopts a short α-helix conformation S316-F322 in the NMR structure. The structural rearrangement of $VP7_{61}$ seems to confer membranotropic properties to that peptide, consisting in membrane destabilization, while the full protein VP7 does not. Thus, VP7 is not only involved in the control of the transcriptional activity of the rotavirus particles [75,76] and in cell attachment by interacting with integrin receptors [20,67], but could also be implicated in other biological processes like membrane permeabilization by release of membranotropic fragments. These findings on VP7 could underline the economy developed by the viruses to use the same protein for different functions and minimize the size of their genome and of the viral capsid, and they could be generalized to other non-enveloped viruses, such as nodaviruses [77], reoviruses [78], birnaviruses [31] and picobirnaviruses [79].

We have recently shown that pep46, one of the peptides present in the virus capsid of the birnavirus, was able to induce pores into membranes as an intermediate step of the birnavirus-penetration pathway [31]. Pep46 forms a long amphipathic helix that inserts into the membrane with its axis parallel to the surface of the membrane, during the first step of pore formation [31]. We have shown that $VP7_{61}$, a peptide isolated from VP7 changes its structure, inserts into artificial membranes and induces their permeabilization. We can speculate that since rotaviruses bind trypsin [80], VP7 peptides may be produced when the viruses enter the cell and thus participate to the process used by rotaviruses to cross membranes. Such an assertion still requires the demonstration that peptides containing the amphipathic domain T280-M310 are produced during rotavirus infection. Because cells are infected by a reduced number of viruses, with an average number of viruses per cell close to 1 or lower, under these experimental conditions it is difficult to detect the virus particle. Thus, the physiological relevance of our findings remains to be proven and does not allow us to claim a role of this peptide in the mechanism of virus infectivity. Despite this, additional techniques used in this study to elucidate the structure strengthen our conclusions on the structure adopted by the peptide. This work contains information that we believe will be useful to other researchers in the field.

Supplementary data to this article can be found online at http://dx.doi.org/10.1016/j.bbamem.2014.04.005.

Acknowledgements

We thank Dr D. Poncet for the use of his facilities. This project was supported by CNRS, INRA and grants from the ANR, including postdoctoral fellowships awarded to SL (ANR-06-BLAN-0103-01) and a Ph.D. grant from Région Ile-de-France to SE (DIM-Malinf maladies infectieuses, 2009).

References

[1] A.Z. Kapikian, R.M. Chanock, Rotaviruses, in: K.D.N., B.N. Fields, P.M. Howley, R.M. Chanock, J.L. Melnick, T.P. Monath, B. Roizman, S.E. Straus (Eds.), Fields virologyLippincott-Raven, Philadelphia, Pa, 1996, pp. 1657–1708.
[2] M.K. Estes, Rotaviruses and their replication, in: K.D.N., B.N. Fields, P.M. Howley, R.M. Chanock, J.L. Melnick, T.P. Monath, B. Roizman, S.E. Straus (Eds.), Fields VirologyLippincott-Raven, Philadelphia, Pa, 1996, pp. 1625–1655.
[3] J.B. Pesavento, S.E. Crawford, M.K. Estes, B.V. Prasad, Rotavirus proteins: structure and assembly, Curr. Top. Microbiol. Immunol. 309 (2006) 189–219.
[4] B.V. Prasad, W. Chiu, Structure of rotavirus, Curr. Top. Microbiol. Immunol. 185 (1994) 9–29.
[5] A. Roseto, J. Escaig, E. Delain, J. Cohen, R. Scherrer, Structure of rotaviruses as studied by the freeze-drying technique, Virology 98 (1979) 471–475.
[6] B.V. Prasad, G.J. Wang, J.P. Clerx, W. Chiu, Three-dimensional structure of rotavirus, J. Mol. Biol. 199 (1988) 269–275.
[7] B.V. Prasad, J.W. Burns, E. Marietta, M.K. Estes, W. Chiu, Localization of VP4 neutralization sites in rotavirus by three-dimensional cryo-electron microscopy, Nature 343 (1990) 476–479.
[8] M. Yeager, J.A. Berriman, T.S. Baker, A.R. Bellamy, Three-dimensional structure of the rotavirus haemagglutinin VP4 by cryo-electron microscopy and difference map analysis, Embo J. 13 (1994) 1011–1018.
[9] J.A. Lawton, M.K. Estes, B.V. Prasad, Comparative structural analysis of transcriptionally competent and incompetent rotavirus-antibody complexes, Proc. Natl. Acad. Sci. U. S. A. 96 (1999) 5428–5433.
[10] M.K. Estes, D.Y. Graham, B.B. Mason, Proteolytic enhancement of rotavirus infectivity: molecular mechanisms, J. Virol. 39 (1981) 879–888.
[11] P. Nandi, A. Charpilienne, J. Cohen, Interaction of rotavirus particles with liposomes, J. Virol. 66 (1992) 3363–3367.
[12] E. Denisova, W. Dowling, R. LaMonica, R. Shaw, S. Scarlata, F. Ruggeri, E.R. Mackow, Rotavirus capsid protein VP5* permeabilizes membranes, J. Virol. 73 (1999) 3147–3153.
[13] L. Fiore, H.B. Greenberg, E.R. Mackow, The VP8 fragment of VP4 is the rhesus rotavirus hemagglutinin, Virology 181 (1991) 553–563.
[14] E.C. Settembre, J.Z. Chen, P.R. Dormitzer, N. Grigorieff, S.C. Harrison, Atomic model of an infectious rotavirus particle, Embo J. 30 (2011) 408–416.
[15] P.R. Dormitzer, Z.Y. Sun, G. Wagner, S.C. Harrison, The rhesus rotavirus VP4 sialic acid binding domain has a galectin fold with a novel carbohydrate binding site, Embo J. 21 (2002) 885–897.
[16] P.R. Dormitzer, E.B. Nason, B.V. Prasad, S.C. Harrison, Structural rearrangements in the membrane penetration protein of a non-enveloped virus, Nature 430 (2004) 1053–1058.
[17] S.T. Aoki, E.C. Settembre, S.D. Trask, H.B. Greenberg, S.C. Harrison, P.R. Dormitzer, Structure of rotavirus outer-layer protein VP7 bound with a neutralizing Fab, Science 324 (2009) 1444–1447.
[18] P.R. Dormitzer, H.B. Greenberg, S.C. Harrison, Purified recombinant rotavirus VP7 forms soluble, calcium-dependent trimers, Virology 277 (2000) 420–428.
[19] B.S. Coulson, S.L. Londrigan, D.J. Lee, Rotavirus contains integrin ligand sequences and a disintegrin-like domain that are implicated in virus entry into cells, Proc. Natl. Acad. Sci. U. S. A. 94 (1997) 5389–5394.
[20] K.L. Graham, P. Halasz, Y. Tan, M.J. Hewish, Y. Takada, E.R. Mackow, M.K. Robinson, B.S. Coulson, Integrin-using rotaviruses bind alpha2beta1 integrin alpha2 I domain via VP4 DGE sequence and recognize alphaXbeta2 and alphaVbeta3 by using VP7 during cell entry, J. Virol. 77 (2003) 9969–9978.
[21] S. Zarate, M.A. Cuadras, R. Espinosa, P. Romero, K.O. Juarez, M. Camacho-Nuez, C.F. Arias, S. Lopez, Interaction of rotaviruses with Hsc70 during cell entry is mediated by VP5, J. Virol. 77 (2003) 7254–7260.
[22] L. Hu, S.E. Crawford, R. Czako, N.W. Cortes-Penfield, D.F. Smith, J. Le Pendu, M.K. Estes, B.V. Prasad, Cell attachment protein VP8* of a human rotavirus specifically interacts with A-type histo-blood group antigen, Nature 485 (2012) 256–259.
[23] P. Huang, M. Xia, M. Tan, W. Zhong, C. Wei, L. Wang, A. Morrow, X. Jiang, Spike protein VP8* of human rotavirus recognizes histo-blood group antigens in a type-specific manner, J. Virol. 86 (2012) 4833–4843.
[24] H. Suzuki, S. Kitaoka, T. Konno, T. Sato, N. Ishida, Two modes of human rotavirus entry into MA 104 cells, Arch. Virol. 85 (1985) 25–34.
[25] C. Sanchez-San Martin, T. Lopez, C.F. Arias, S. Lopez, Characterization of rotavirus cell entry, J. Virol. 78 (2004) 2310–2318.
[26] J.D. Yoder, P.R. Dormitzer, Alternative intermolecular contacts underlie the rotavirus VP5* two- to three-fold rearrangement, Embo J. 25 (2006) 1559–1568.

[27] S.D. Trask, I.S. Kim, S.C. Harrison, P.R. Dormitzer, A rotavirus spike protein conformational intermediate binds lipid bilayers, J. Virol. 84 (2010) 1764–1770.
[28] A. Odegard, M. Banerjee, J.E. Johnson, Flock house virus: a model system for understanding non-enveloped virus entry and membrane penetration, Curr. Top. Microbiol. Immunol. 343 (2010) 1–22.
[29] J.E. Johnson, P.K. Vogt, Cell entry by non-enveloped viruses, Curr. Top. Microbiol. Immunol. 343 (2010) v–vii.
[30] L.F. Maia, M.R. Soares, A.P. Valente, F.C. Almeida, A.C. Oliveira, A.M. Gomes, M.S. Freitas, A. Schneemann, J.E. Johnson, J.L. Silva, Structure of a membrane-binding domain from a non-enveloped animal virus: insights into the mechanism of membrane permeability and cellular entry, J. Biol. Chem. 281 (2006) 29278–29286.
[31] M. Galloux, S. Libersou, I.D. Alves, R. Marquant, G.F. Salgado, H. Rezaei, J. Lepault, B. Delmas, S. Bouaziz, N. Morellet, NMR structure of a viral peptide inserted in artificial membranes: a view on the early steps of the birnavirus entry process, J. Biol. Chem. 285 (2010) 19409–19421.
[32] M. Galloux, S. Libersou, N. Morellet, S. Bouaziz, B. Da Costa, M. Ouldali, J. Lepault, B. Delmas, Infectious bursal disease virus, a non-enveloped virus, possesses a capsid-associated peptide that deforms and perforates biological membranes, J. Biol. Chem. 282 (2007) 20774–20784.
[33] T. Ivanovic, M.A. Agosto, L. Zhang, K. Chandran, S.C. Harrison, M.L. Nibert, Peptides released from reovirus outer capsid form membrane pores that recruit virus particles, Embo J. 27 (2008) 1289–1298.
[34] L. Zhang, M.A. Agosto, T. Ivanovic, D.S. King, M.L. Nibert, S.C. Harrison, Requirements for the formation of membrane pores by the reovirus myristoylated micro1N peptide, J. Virol. 83 (2009) 7004–7014.
[35] L. Zhang, K. Chandran, M.L. Nibert, S.C. Harrison, Reovirus mu1 structural rearrangements that mediate membrane penetration, J. Virol. 80 (2006) 12367–12376.
[36] R. Mani, S.D. Cady, M. Tang, A.J. Waring, R.I. Lehrer, M. Hong, Membrane-dependent oligomeric structure and pore formation of a beta-hairpin antimicrobial peptide in lipid bilayers from solid-state NMR, Proc. Natl. Acad. Sci. U. S. A. 103 (2006) 16242–16247.
[37] C. Snider, S. Jayasinghe, K. Hristova, S.H. White, MPEx: a tool for exploring membrane proteins, Protein Sci. 18 (2009) 2624–2628.
[38] B. Rost, PHD: predicting one-dimensional protein structure by profile-based neural networks, Methods Enzymol. 266 (1996) 525–539.
[39] C. Combet, C. Blanchet, C. Geourjon, G. Deleage, NPS@: network protein sequence analysis, Trends Biochem. Sci. 25 (2000) 147–150.
[40] P. Mueller, D.O. Rudin, Resting and action potentials in experimental bimolecular lipid membranes, J. Theor. Biol. 18 (1968) 222–258.
[41] Z. Salamon, D. Huang, W.A. Cramer, G. Tollin, Coupled plasmon-waveguide resonance spectroscopy studies of the cytochrome b6f/plastocyanin system in supported lipid bilayer membranes, Biophys. J. 75 (1998) 1874–1885.
[42] I.D. Alves, Z. Salamon, E. Varga, H.I. Yamamura, G. Tollin, V.J. Hruby, Direct observation of G-protein binding to the human delta-opioid receptor using plasmon-waveguide resonance spectroscopy, J. Biol. Chem. 278 (2003) 48890–48897.
[43] Z. Salamon, G. Tollin, Graphical analysis of mass and anisotropy changes observed by plasmon-waveguide resonance spectroscopy can provide useful insights into membrane protein function, Biophys. J. 86 (2004) 2508–2516.
[44] H.P. Ta, K. Berthelot, B. Coulary-Salin, S. Castano, B. Desbat, P. Bonnafous, O. Lambert, I. Alves, C. Cullin, S. Lecomte, A yeast toxic mutant of HET-s amyloid disrupts membrane integrity, Biochim. Biophys. Acta 1818 (9) (2012) 2325–2334.
[45] G.F. Salgado, R. Marquant, A. Vogel, I.D. Alves, S.E. Feller, N. Morellet, S. Bouaziz, Structural studies of HIV-1 Gag p6ct and its interaction with Vpr determined by solution nuclear magnetic resonance, Biochemistry 48 (2009) 2355–2367.
[46] I.D. Alves, C. Bechara, A. Walrant, Y. Zaltsman, C.Y. Jiao, S. Sagan, Relationships between membrane binding, affinity and cell internalization efficacy of a cell-penetrating peptide: penetratin as a case study, PLoS One 6 (2011) e24096.
[47] R.J. Lee, S. Wang, M.J. Turk, P.S. Low, The effects of pH and intraliposomal buffer strength on the rate of liposome content release and intracellular drug delivery, Biosci. Rep. 18 (1998) 69–78.
[48] A. Derome, M. Williamson, 2D homonuclear shift correlation phase sensitive using TPPI with double quantum filter phase cycle, J. Magn. Reson. 88 (1990) 177–185.
[49] C. Griesinger, G. Otting, K. Wurthrich, R.R. Ernst, Clean Tocsy for H-1 spin system-identification in macromolecules, J. Am. Chem. Soc. (1988) 7870–7872.
[50] J. Jeener, B.H. Meier, P. Bachmann, R.R. Ernst, investigation of exchange processes by 2-dimensional NMR-spectroscopy, J. Chem. Phys. 71 (1979) 4546–4553.
[51] W.F. Vranken, W. Boucher, T.J. Stevens, R.H. Fogh, A. Pajon, M. Llinas, E.L. Ulrich, J.L. Markley, J. Ionides, E.D. Laue, The CCPN data model for NMR spectroscopy: development of a software pipeline, Proteins 59 (2005) 687–696.
[52] K. Wuthrich, NMR of proteins and nucleic acids, Wiley/Interscince, USA, 1986.
[53] C.D. Schwieters, J.J. Kuszewski, N. Tjandra, G.M. Clore, The Xplor-NIH NMR molecular structure determination package, J. Magn. Reson. 160 (2003) 65–73.
[54] S. Bourbigot, H. Beltz, J. Denis, N. Morellet, B.P. Roques, Y. Mely, S. Bouaziz, The C-terminal domain of the HIV-1 regulatory protein Vpr adopts an antiparallel dimeric structure in solution via its leucine-zipper-like domain, Biochem. J. 387 (2005) 333–341.
[55] R.A. Laskowski, J.A. Rullmannn, M.W. MacArthur, R. Kaptein, J.M. Thornton, AQUA and PROCHECK-NMR: programs for checking the quality of protein structures solved by NMR, J. Biomol. NMR 8 (1996) 477–486.
[56] A.T. Brunger, P.D. Adams, G.M. Clore, W.L. DeLano, P. Gros, R.W. Grosse-Kunstleve, J.S. Jiang, J. Kuszewski, M. Nilges, N.S. Pannu, R.J. Read, L.M. Rice, T. Simonson, G.L. Warren, Crystallography & NMR system: a new software suite for macromolecular structure determination, Acta Crystallogr. D Biol. Crystallogr. 54 (1998) 905–921.
[57] B. Bardiaux, T. Malliavin, M. Nilges, ARIA for solution and solid-state NMR, Methods Mol. Biol. 831 (2012) 453–483.
[58] A. Charpilienne, M.J. Abad, F. Michelangeli, F. Alvarado, M. Vasseur, J. Cohen, M.C. Ruiz, Solubilized and cleaved VP7, the outer glycoprotein of rotavirus, induces permeabilization of cell membrane vesicles, J. Gen. Virol. 78 (Pt 6) (1997) 1367–1371.
[59] D.T. Jones, Protein secondary structure prediction based on position-specific scoring matrices, J. Mol. Biol. 292 (1999) 195–202.
[60] I.D. Alves, I. Correia, C.Y. Jiao, E. Sachon, S. Sagan, S. Lavielle, G. Tollin, G. Chassaing, The interaction of cell-penetrating peptides with lipid model systems and subsequent lipid reorganization: thermodynamic and structural characterization, J. Pept. Sci. 15 (2009) 200–209.
[61] G.F. Salgado, A. Vogel, R. Marquant, S.E. Feller, S. Bouaziz, I.D. Alves, The role of membranes in the organization of HIV-1 Gag p6 and Vpr: p6 shows high affinity for membrane bilayers which substantially increases the interaction between p6 and Vpr, J. Med. Chem. 52 (2009) 7157–7162.
[62] N. Pendem, C. Douat, P. Claudon, M. Laguerre, S. Castano, B. Desbat, D. Cavagnat, E. Ennifar, B. Kauffmann, G. Guichard, Helix-forming propensity of aliphatic urea oligomers incorporating noncanonical residue substitution patterns, J. Am. Chem. Soc. 135 (2013) 4884–4892.
[63] B.M. Burkhart, R.M. Gassman, D.A. Langs, W.A. Pangborn, W.L. Duax, V. Pletnev, Gramicidin D conformation, dynamics and membrane ion transport, Biopolymers 51 (1999) 129–144.
[64] V.Y. Orekhov, P.V. Dubovskii, H. Yamada, K. Akasaka, A.S. Arseniev, Pressure effect on the dynamics of an isolated alpha-helix studied by 15 N-1H NMR relaxation, J. Biomol. NMR 17 (2000) 257–263.
[65] V.S. Pashkov, I.V. Maslennikov, L.D. Tchikin, R.G. Efremov, V.T. Ivanov, A.S. Arseniev, Spatial structure of the M2 transmembrane segment of the nicotinic acetylcholine receptor alpha-subunit, FEBS Lett. 457 (1999) 117–121.
[66] A.T. Brunger, P.D. Adams, L.M. Rice, Recent developments for the efficient crystallographic refinement of macromolecular structures, Curr. Opin. Struct. Biol. 8 (1998) 606–611.
[67] S. Zarate, P. Romero, R. Espinosa, C.F. Arias, S. Lopez, VP7 mediates the interaction of rotaviruses with integrin alphavbeta3 through a novel integrin-binding site, J. Virol. 78 (2004) 10839–10847.
[68] F.M. Ruggeri, H.B. Greenberg, Antibodies to the trypsin cleavage peptide VP8 neutralize rotavirus by inhibiting binding of virions to target cells in culture, J. Virol. 65 (1991) 2211–2219.
[69] M.A. Cuadras, C.F. Arias, S. Lopez, Rotaviruses induce an early membrane permeabilization of MA104 cells and do not require a low intracellular Ca2+ concentration to initiate their replication cycle, J. Virol. 71 (1997) 9065–9074.
[70] F. Liprandi, Z. Moros, M. Gerder, J.E. Ludert, F.H. Pujol, M.C. Ruiz, F. Michelangeli, A. Charpilienne, J. Cohen, Productive penetration of rotavirus in cultured cells induces coentry of the translation inhibitor alpha-sarcin, Virology 237 (1997) 430–438.
[71] D. Silva-Ayala, T. Lopez, M. Gutierrez, N. Perrimon, S. Lopez, C.F. Arias, Genome-wide RNAi screen reveals a role for the ESCRT complex in rotavirus cell entry, Proc. Natl. Acad. Sci. U. S. A. 110 (2013) 10270–10275.
[72] B. Bechinger, J.M. Ruysschaert, E. Goormaghtigh, Membrane helix orientation from linear dichroism of infrared attenuated total reflection spectra, Biophys. J. 76 (1999) 552–563.
[73] Y. Shai, Mechanism of the binding, insertion and destabilization of phospholipid bilayer membranes by alpha-helical antimicrobial and cell non-selective membranelytic peptides, Biochim. Biophys. Acta 1462 (1999) 55–70.
[74] D.I. Chan, E.J. Prenner, H.J. Vogel, Tryptophan- and arginine-rich antimicrobial peptides: structures and mechanisms of action, Biochim. Biophys. Acta 1758 (2006) 1184–1202.
[75] J.Z. Chen, E.C. Settembre, S.T. Aoki, X. Zhang, A.R. Bellamy, P.R. Dormitzer, S.C. Harrison, N. Grigorieff, Molecular interactions in rotavirus assembly and uncoating seen by high-resolution cryo-EM, Proc. Natl. Acad. Sci. U. S. A. 106 (2009) 10644–10648.
[76] S. Libersou, X. Siebert, M. Ouldali, L.F. Estrozi, J. Navaza, A. Charpilienne, P. Garnier, D. Poncet, J. Lepault, Geometric mismatches within the concentric layers of rotavirus particles: a potential regulatory switch of viral particle transcription activity, J. Virol. 82 (2008) 2844–2852.
[77] D.T. Bong, C. Steinem, A. Janshoff, J.E. Johnson, M. Reza Ghadiri, A highly membrane-active peptide in Flock House virus: implications for the mechanism of nodavirus infection, Chem. Biol. 6 (1999) 473–481.
[78] M.A. Agosto, T. Ivanovic, M.L. Nibert, Mammalian reovirus, a nonfusogenic nonenveloped virus, forms size-selective pores in a model membrane, Proc. Natl. Acad. Sci. U. S. A. 103 (2006) 16496–16501.
[79] S. Duquerroy, B. Da Costa, C. Henry, A. Vigouroux, S. Libersou, J. Lepault, J. Navaza, B. Delmas, F.A. Rey, The picobirnavirus crystal structure provides functional insights into virion assembly and cell entry, Embo J. 28 (2009) 1655–1665.
[80] Y. Benureau, J.C. Huet, A. Charpilienne, D. Poncet, J. Cohen, Trypsin is associated with the rotavirus capsid and is activated by solubilization of outer capsid proteins, J. Gen. Virol. 86 (2005) 3143–3151.